Draft version October 14, 2018
Typeset using LaTeX **twocolumn** style in AASTeX62

Predicting the Rossby number in convective experiments

Evan H. Anders,[1,2] Cathryn M. Manduca,[3] Benjamin P. Brown,[3] Jeffrey S. Oishi,[3] and Geoffrey M. Vasil[4]

[1] *Dept. Astrophysical & Planetary Sciences, University of Colorado – Boulder, Boulder, CO 80309, USA*
[2] *Laboratory for Atmospheric and Space Physics, Boulder, CO 80303, USA*
[3] *Department of Physics and Astronomy, Bates College, Lewiston, ME 04240, USA*
[4] *University of Sydney School of Mathematics and Statistics, Sydney, NSW 2006, Australia*

(Received October 14, 2018; Revised ??; Accepted ??)

Submitted to ApJL

ABSTRACT

The Rossby number is a crucial parameter describing the degree of rotational constraint on the convective dynamics in stars and planets. However, it is not an input to computational models of convection but must be measured ex post facto. Here, we report the discovery of a new quantity, the Predictive Rossby number, which is both tightly correlated with the Rossby number and specified in terms of common inputs to numerical models. The Predictive Rossby number can be specified independent of Rayleigh number, allowing suites of numerical solutions to separate the degree of rotational constraint from the strength of the driving convection. We examine the scaling of convective transport in terms of the Nusselt number and the degree of turbulence in terms of the Reynolds number of the flow. Finally, we describe the boundary layers as a function of increasing turbulence at constant Rossby number.

Keywords: convection — rotation — turbulence

1. INTRODUCTION

Rotation influences the dynamics of convective flows in stellar and planetary atmospheres. Many studies on the fundamental nature of rotating convection in both laboratory and numerical settings have provided great insight into the properties of convection in both the rapidly rotating regime (**???**) and the transition to the rotationally unconstrained regime (**???**). The scaling behavior of heat transport, the nature of convective flow structures, and the importance of boundary layer-bulk interactions in driving dynamics are well known. Yet, we do know of any simple procedure for predicting the magnitude of flow gradients purely from experimental control parameters; such a bulk rotation rate and thermal input.

In the astrophysical context, many studies of rotating convection have investigated questions inspired by the solar dynamo (**????????**). Even when these simulations nominally rotate at the solar rate, they frequently produce distinctly different behaviors than the true Sun, such as anti-solar differential rotation profiles. It seems that these differences occur because the simulation produce less rotationally constrained stated than the true sun. The influence of rotation results from the local shear gradients, and these are not direct input parameters. Recent simulations predict significant rotational influence in the deep solar interior, which can drastically affect flows throughout the solar convection zone(**??**). In the planetary context, the balance between magnetic and rotational forces likely leads to the observed differences between ice giant and gas giant dynamos in our solar system (**?**). In particular, **?** suggest that many studies of planetary systems have over-emphasized the importance of magnetism compared to rotation.

In short, simulations must have the proper rotational balance if they are to explain the behavior of astrophys-

Corresponding author: Evan H. Anders
evan.anders@colorado.edu

ical objects. The degree of rotational influence is best assessed by the ratio between nonlinear advection magnitude, and the linear Coriolis accelerations. The *Rossby number* provides the standard way to measure this ratio,

$$\mathrm{Ro} \equiv \frac{|\nabla \times \boldsymbol{u}|}{2\Omega} \sim \frac{|(\nabla \times \boldsymbol{u}) \times \boldsymbol{u}|}{|2\Omega \times \boldsymbol{u}|} \quad (1)$$

where Ω denotes the bulk rotation rate. Many proxies for the dynamical Rossby number exist that are based solely on input parameters; most notably the *convective* Rossby number. However, all proxies produce imperfect predictions for the true dynamically relevant quantity.

> *In the letter, we demonstrate an emperical method of predicting the output Rossby number of convection in a simple stratified system.*

In **?** (hereafter **?**), we studied non-rotating compressible convection without magnetic fields in polytropic atmospheres. In this work, we extend **?** to rotationally-influenced, f-plane atmospheres (e.g. **???**). We determine how the input parameters we studied previously, controlling the Mach and Reynolds numbers of the evolved flows, couple with the the Taylor number (Ta, **?**), which sets the magnitude of the rotational vector.

In section 2, we describe our experiment and paths through parameter space. In section 3, we present the results of our experiments and in section 4 we offer concluding remarks.

2. EXPERIMENT

We study fully compressible, stratified convection under precisely the same atmospheric model as in **?**, but here we have included rotation. We study polytropic atmospheres with $n_\rho = 3$ density scale heights and a superadiabatic excess of $\epsilon = 10^{-4}$ such that flows are at low Mach number. We study a domain in which the gravity, $\boldsymbol{g} = -g\hat{z}$, and rotational vector, $\boldsymbol{\Omega} = \Omega\hat{z}$, are antiparallel (as in e.g., **??**).

We evolve the velocity ($\boldsymbol{u}$), temperature (T), and log density ($\ln\rho$) in the same form presented in **?**, with the addition of the Coriolis term, $2\boldsymbol{\Omega} \times \boldsymbol{u}$, to the left-hand side of the momentum equation. We impose impenetrable, stress-free, fixed-temperature boundary conditions at the top and bottom of the domain.

We set the kinematic viscosity (ν), thermal diffusivity (χ), and strength of rotation (Ω) at the top of the domain by the Rayleigh number (Ra), Prandtl number (Pr), and Taylor number (Ta),

$$\mathrm{Ra} = \frac{gL_z^3\Delta S/c_P}{\nu\chi}, \quad \mathrm{Pr} = \frac{\nu}{\chi}, \quad \mathrm{Ta} = \left(\frac{2\Omega L_z^2}{\nu}\right)^2, \quad (2)$$

where L_z is the depth of the domain, $\Delta S \propto \epsilon n_\rho$ is the specific entropy difference between $z = 0$ and $z = L_z$, and the specific heat at constant pressure is c_P. Throughout this work we set $\mathrm{Pr} = 1$.

The *convective* Rossby number has provided (e.g., **??**) a common proxy (based on input parameters) for the degree of rotational constraint

$$\mathrm{Ro}_c = \sqrt{\frac{\mathrm{Ra}}{\mathrm{Pr\,Ta}}} = \frac{1}{2\Omega}\sqrt{\frac{g\,\Delta S}{c_p L_z}} \quad (3)$$

This parameter measures the importance of buoyancy relative to rotation without involving dissipation. We show that true Rossby number defined in equation 1 depends nonlinearly on Ro_c.

The wavenumber of convective onset increases such that, $k_{\mathrm{crit}} \sim \mathrm{Ta}^{1/6}$ (approximately), (**??**). We study 3D Cartesian convective domains with horizontal extents of $x, y = [0, 4(2\pi/k_{\mathrm{crit}})]$. We evolve our simulations using the Dedalus[1] pseudospectral framework, and our numerical methods are identical to those presented in **?**.

The critical value of Ra at which convection onsets also depends on Ta (see the black line in figure 1a); roughly according to $\mathrm{Ra}_{\mathrm{crit}} \sim \mathrm{Ta}^{2/3}$ **?**. Even taking into account of linear theory, the nonlinear dependence of the evolved fluid flows on the input parameters predict the rotational constraint very challenging. We will explore three paths through Ra-Ta space:

$$\mathrm{Ra} = \begin{cases} \mathcal{S}\,\mathrm{Ra}_{\mathrm{crit}}(\mathrm{Ta}), & \text{(I)} \\ (\mathrm{Ro}_c)^2\,\mathrm{Pr\,Ta}, & \text{(II)} \\ (\mathrm{Ro}_*)^2\,\mathrm{Pr\,Ta}^{3/4} & \text{(III)}. \end{cases} \quad (4)$$

Paths on constraint I are at constant supercriticality, $\mathcal{S} \equiv \mathrm{Ra}/\mathrm{Ra}_{\mathrm{crit}}$ (blue dash-dot line in figure 1a). Paths on constraint II are at a constant value of the classic Ro_c (green dashed line in figure 1a). Paths on constraint III (e.g., orange solid line in figure 1a) set constant a ratio which we call the "Predictive Rossby Number,"

$$\mathrm{Ro}_* = \sqrt{\frac{\mathrm{Ra}}{\mathrm{Pr\,Ta}^{3/4}}} = \frac{1}{2\Omega}\sqrt{\frac{g\,\Delta S}{c_p L_*}} \quad (5)$$

To our knowledge, these paths have not been reported in the literature. The importance of the predictive Rossby number implies the importance of a dynamical length scale,

$$L_* \sim \frac{L_z}{\mathrm{Ta}^{1/4}} \quad (6)$$

[1] http://dedalus-project.org/

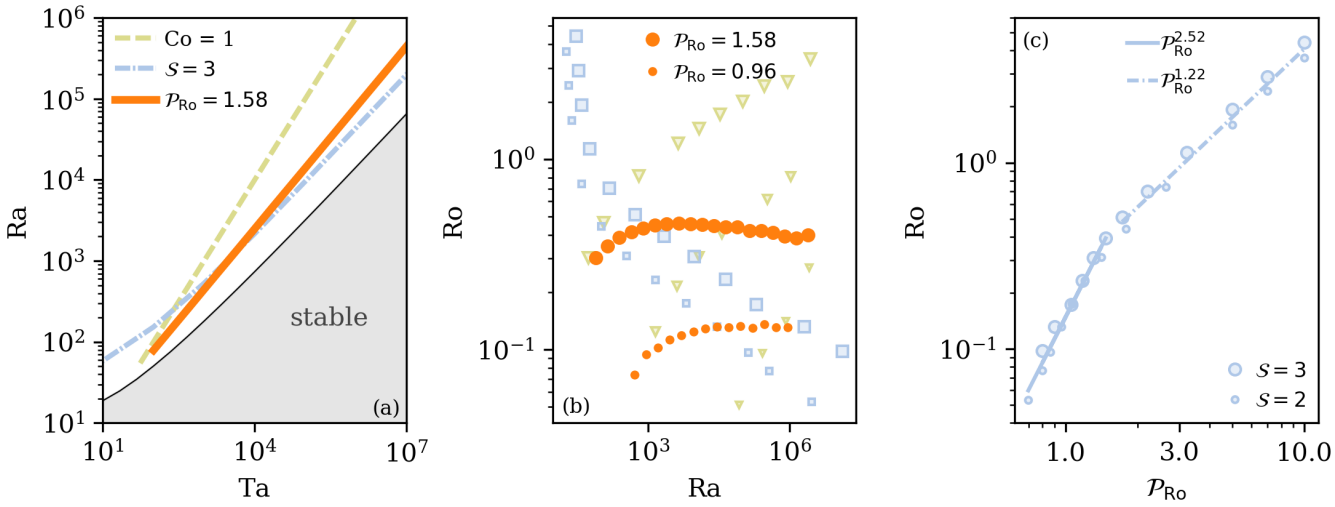

Figure 1. (a) The critical Rayleigh number, as a function of the Taylor number, is plotted as a solid black line. The grey shaded region is subcritical, and rotation supresses convection there. Paths of constant Convective Rossby Number (Ro_c, green dashed line), constant supercriticality ($\mathcal{S}$, blue dash-dot line), and constant Ro_*(orange solid line) are shown through parameter space. (b) Evolved Ro is plotted vs. Ra along paths of Ro_*= [1.58, 0.96] for [big, small] orange circles. For comparison, paths of constant $\mathcal{S}$ (blue squares, $\mathcal{S} = [3, 2]$ for [big, small] squares) and constant Ro_c (green triangles, Ro_c = [1, 0.3, 0.1] for [big, medium, small] triangles) are shown. Ro is roughly constant for a constant Ro_*, particularly for the low-Ro, $\mathrm{Ro}_* = 0.96$ case, but changes drastically at constant Ro_c or $\mathcal{S}$. (c) The scaling of Ro with Ro_* is shown for $\mathcal{S} = [2, 3]$. At low Ro, both supercriticalities collapse onto a common scaling law of $\mathrm{Ro} \propto \mathrm{Ro}_*^{2.52}$. For rotationally unconstrained flows, we measure $\mathrm{Ro} \propto \mathrm{Ro}_*^{1.22}$, and the value of Ro varies with $\mathcal{S}$.

This differs noticeably from the anticipated onset length scale

$$L_{\rm crit.} \sim \frac{L_z}{\mathrm{Ta}^{1/6}}. \tag{7}$$

Length-scale correction of the form of equation 6 have been proposed in systems with no-slip boundary conditions and Ekman pumping effects. However, we see this scale in a system with stress-free boundaries and ostensibly no significant Ekman fluxes.

3. RESULTS

In figure 1a, the value of $\mathrm{Ra}_{\rm crit}$ is shown as a function of Ta, as calculated by a linear instability analysis. A sample path for each criterion in equation 4 through this parameter space is shown. In figure 1b, we display the scaling of Ro with increasing Ra along various paths through parameter space. We find that Ro increases on constant Ro_cpaths, decreases on constant $\mathcal{S}$ paths, and remains roughly constant along constant Ro_* paths. In figure 1c, the behavior of Ro is shown as a function of Ro_* at constant $\mathcal{S}$. At low Ro and Ro_*, in the rotationally constrained regime, the two parameters follow a scaling of $\mathrm{Ro} \propto \mathrm{Ro}_*^{2.52}$. At higher Ro in the rotationally unconstrained regime, this scaling breaks down to a $\mathrm{Ro} \propto \mathrm{Ro}_*^{1.22}$ law, with some offset at different values of $\mathcal{S}$.

In figure 2, sample snapshots of the evolved entropy field in the x-y plane near the top of the domain are shown. In the left panel is a rotationally unconstrained flow at moderately high Ro, and Ro decreases into the rotationally constrained regime from left to right. As Ro decreases, the classic granular structure of convection (see e.g., figure 2 in **?**) gives way to vortical columns of convection, as seen in rapidly rotating Rayleigh-Bénard convection (**?**). The select cases displayed in figure 2 have an evolved volume-averaged $\mathrm{Re} \sim 200$.

We measure the Nusselt number (Nu), which quantifies heat transport in a convective solution, as we did in **?**. In figure 3a, we show how Nu scales as a function of Ra at fixed Ro_*. When $\mathrm{Ro} \sim 0.1$, we find a scaling of $\mathrm{Nu} \propto \mathrm{Ra}^{0.27}$. This is reminiscent of classic scaling laws (e.g., $\mathrm{Ra}^{2/7}$) in non-rotating Rayleigh-Bénard convection (**?**). This suggests that changes in heat transport at constant $\mathrm{Ro}_*$are driven by changes in the boundary layer structure with increasing Ra. In figure 3b, we plot the RMS Reynold's number ($\mathrm{Re} = |u|L_z/\nu$) as a function of Ra at fixed Ro_*, and find that $\mathrm{Re} \propto \mathrm{Ra}^{0.47}$ in the rotationally constrained regime, which is almost precisely the $\mathrm{Re} \propto \mathrm{Ra}^{1/2}$ scaling measured in the non-rotating regime in **?**.

Figure 4 shows time- and horizontally-averaged profiles of Ro and the z-component of the specific entropy gradient, $(\nabla s)_z$. Figures 4a&b show these profiles for $\mathrm{Ro}_* = 0.96$, while Figures 4c&d show these profiles for $\mathrm{Ro}_* = 1.58$. The transition in profile behavior from low Ra (yellow) to high Ra (purple) is denoted by the

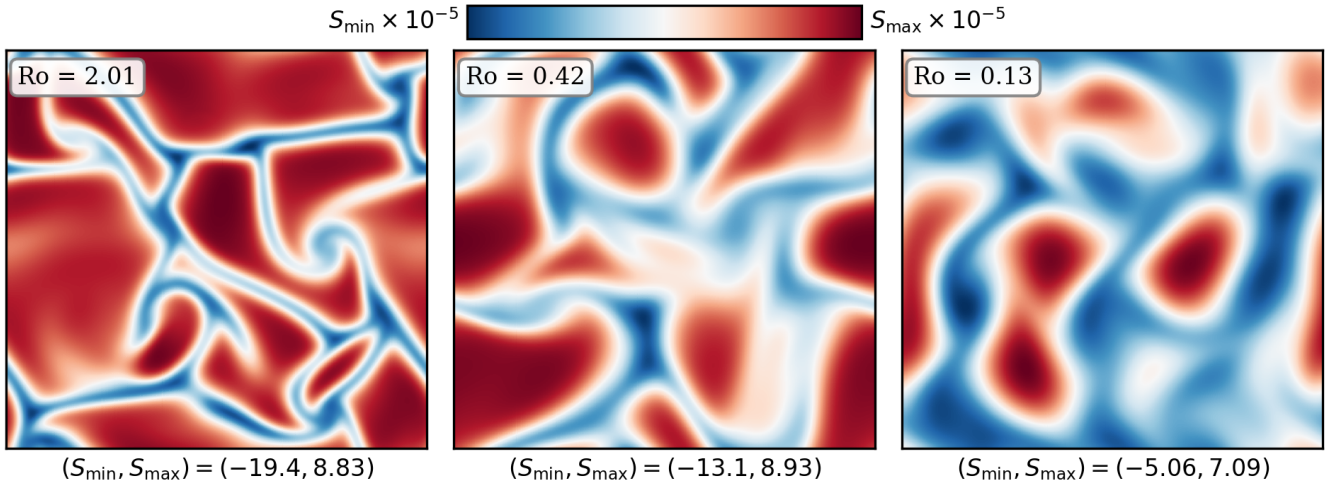

Figure 2. A horizontal slice of the evolved entropy field is plotted at $z = 0.95L_z$ for select simulations. The mean value of entropy at this height has been removed in all cases. All runs displayed here have an evolved volume-averaged Re $\sim$ 200. As Ro decreases from O(1) on the left to O(0.1) on the right, and thus the rotational constraint on the flow increases, significant changes in flow morphology are observed. At Ro = 2.01, convective dynamics are not hugely dissimilar from the non-rotating case where there are large upflows and narrow, fast downflow lanes (see e.g., **?**). As the rotational constraint increases, the granular convective pattern gives way to vortical columns, as seen at Ro = 0.13.

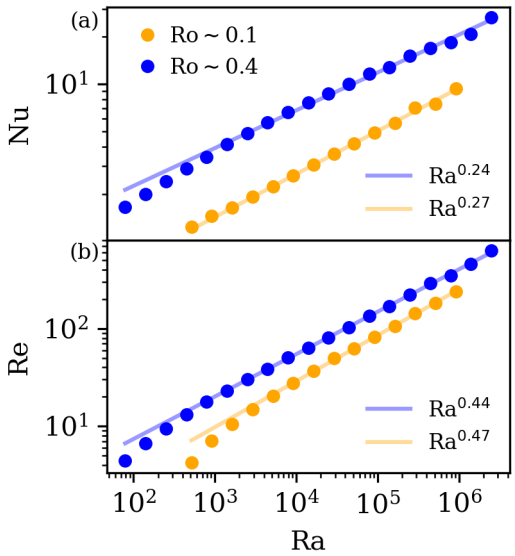

Figure 3. Scaling laws for paths at $\mathrm{Ro}_* = 1.58$ (Ro $\sim$ 0.4) and $\mathrm{Ro}_* = 0.96$ (Ro $\sim$ 0.1) are shown. (a) Evolved Nu vs. Ra. The scaling laws here are very reminiscent of classic Rayleigh-Bénard convection theory (**?**). (b) Evolved Re vs. Ra. The scaling seen here is nearly identical to scalings in nonrotating convection.

color of the profile. As Ra increases at a constant value of Ro_*, both the thermal ($(\nabla s)_z$) and dynamical (Ro) boundary layers become thinner. We measure the thickness of the thermal boundary layer ($\delta_{\nabla s}$) at the top of the domain by measuring where a linear fit within the boundary layer crosses through $(\nabla s)_z = 0$. We ensure by-eye for each profile that this is a reasonable measure of the boundary layer thickness. We measure the thickness of the Ro boundary layer (δ_{Ro}) as the height of the peak value of Ro within the upper half of the domain. In figure 4e, we plot $\delta_{\mathrm{Ro}}/\delta_{\nabla s}$, the ratio of these two boundary layers. As anticipated, the dynamical boundary layer (δ_{Ro}) becomes relatively thinner with respect to the thermal boundary layer ($\delta_{\nabla s}$) as Ro and Ro_* decrease. At $\mathrm{Ro}_* = 1.58$, both boundary layers are approximately equally thick, and so both rotational and advective effects are equally important. On the other hand, in the $\mathrm{Ro}_* = 0.96$, the dynamical boundary layer is half the size of the thermal boundary layer, and rotational effects dominate the dynamics.

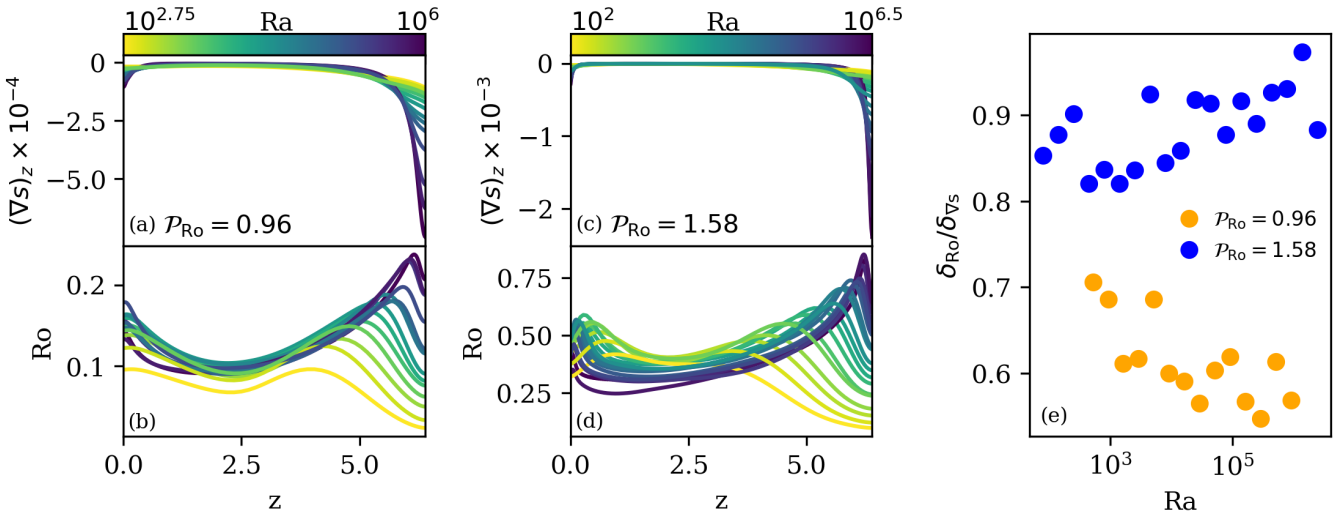

Figure 4. Horizontally-averaged profiles of the z-component of the specific entropy gradient ($(\nabla s)_z$, a) and Rossby number (Ro, b) are shown vs. height for $\mathrm{Ro}_* = 0.96$. Similar profiles are shown in (c) and (d) for $\mathrm{Ro}_* = 1.58$. The color of the profiles denotes the value of Ra, with yellow profiles being at very low Ra and purple at the highest values of Ra studied here. (e) The ratio of the thickness of the dynamical (Ro) boundary layer and thermal ($(\nabla s)_z$) boundary layer is shown for both values of Ro_*at each value of Ra. This ratio is roughly constant across orders of magnitude of Ra.

4. DISCUSSION

In this letter, we studied low-Mach-number, stratified, compressible convection under the influence of rotation. We examined three paths through Ra-Ta space, and showed that in the rotationally constrained regime at low-Ro, the newly-defined Predictive Rossby number, $\mathrm{Ro}_* = \mathrm{Ra}/(\mathrm{Pr}\ \mathrm{Ta}^{3/4})$, determines the value of the evolved Ro. While increasing Ra and holding Ro_* constant, we find scaling laws of heat transport (Nu) and turbulence (Re) that are nearly identical to scaling laws seen in nonrotational convection. We note briefly that the scaling $\mathrm{Ra} \propto \mathrm{Ta}^{3/4}$ is very similar to the theorized boundary between fully rotationally constrained convection and partially constrained convection predicted in Boussinesq theory, of $\mathrm{Ra} \propto \mathrm{Ta}^{4/5}$ (**??**). This $\mathrm{Ta}^{4/5}$ scaling arises through arguments of geostrophic balance in the boundary layers, and is a steeper scaling than the The $\mathrm{Ta}^{3/4}$ scaling present in Ro_*. This suggests that at sufficiently low Ro_*, a suite of simulations across many orders of magnitude of Ra will not only have the same volume-averaged value of Ro (as in Fig. 1b), but will also maintain proper force balances within the boundary layers.

Our results suggest that by choosing the proper value of Ro_*, experimenters can can select the degree of rotational constraint present in their simulations. Once that value is chosen, it is straightforward to increase the turbulent nature of the simulations by increasing Ra, just as in the non-rotating case. Although all the results reported here are for a simple Cartesian geometry with antiparallel gravity and rotation, preliminary 3D spherical simulations suggest that Ro_* also specifies Ro in more complex geometries (Brown et al. 2019 in prep).

EHA acknowledges the support of NASA NESSF (insert fellowship number) and the University of Colorado's George Ellery Hale Graduate Student Fellowship. This work was additionally supported by NASA LWS grant number NNX16AC92G. Computations were conducted with support by the NASA High End Computing (HEC) Program through the NASA Advanced Supercomputing (NAS) Division at Ames Research Center on Pleiades with allocations GID s1647.